Improving the force field description of tyrosine-choline cation-π interactions: QM investigation of phenol-N(Me)$_4^+$ interactions

Hanif M. Khan,[1,2] Cédric Grauffel,[3] Ria Broer,[4] Alexander D. MacKerell Jr.,[5] Remco W. A. Havenith,[4,6,7] and Nathalie Reuter[1,2]

[1] Department of Molecular Biology, University of Bergen, Norway; [2] Computational Biology Unit, Department of Informatics, Bergen, Norway; [3] Institute of Biomedical Sciences, Academia Sinica, Taipei, Taiwan; [4] Zernike Institute for Advanced Materials, University of Groningen, The Netherlands; [5] Department of Pharmaceutical Sciences, University of Maryland, School of Pharmacy, Baltimore, U.S.A; [6] Stratingh Institute for Chemistry, University of Groningen, The Netherlands; [7] Ghent Quantum Chemistry Group, Department of Inorganic and Physical Chemistry, Ghent University, Belgium.

KEYWORDS. choline, tyrosine, cation-π interaction, CHARMM force field, Drude force field, MD simulation

ABSTRACT: Cation-π interactions between tyrosine amino acids and compounds containing a N,N,N-trimethylethanolammonium ($N(CH_3)_3$) are involved in the recognition of histone tails by chromodomains and in the recognition of phosphatidylcholine (PC) phospholipids by membrane-binding proteins. Yet the lack of explicit polarization or charge transfer effects in molecular mechanics force fields raises questions about the reliability of the representation of these interactions in biomolecular simulations. We here investigate the nature of phenol-tetramethylammonium (TMA) interactions using quantum mechanical (QM) calculations, which we also use to evaluate the accuracy of the additive CHARMM36 and polarizable Drude force fields in modeling tyrosine-choline interactions. We show that the potential energy surface (PES) obtained using SAPT2+/aug-cc-pVDZ compares well with the large basis-set CCSD(T) PES when TMA approaches perpendicularly to the phenol ring. Further, the SAPT energy decomposition reveals comparable contributions from electrostatics and dispersion in phenol-TMA interactions. We then compared SAPT2+/aug-cc-pVDZ PES obtained along various approach directions to the corresponding PES obtained with CHARMM and show that the force field accurately reproduces the minimum distances while the interaction energies are underestimated. The use of the polarizable Drude force field significantly improves the interaction energies but decreases the agreement on distances at energy minima. The best agreement between force field and QM PES is obtained by modifying the Lennard-Jones terms for atom pairs involved in the phenol-TMA cation-π interactions. This is further shown to improve the agreement between occupancy of choline-tyrosine cation-π interactions obtained from molecular dynamics simulations of a bilayer-bound bacterial phospholipase and experimental affinity data of the wild-type protein and selected mutants.

INTRODUCTION

Cation-π interactions have long been known to be important for protein structure and stability[1,2] and protein-ligand recognition.[3,4] Within protein structures they typically involve aromatic amino acids (phenylalanine, tyrosine, tryptophan) and arginines, lysines or histidines. They can also involve methylated lysines,[5,6] acetylcholine[7] or nicotine.[8] Cation-π interactions between proteins and choline-containing headgroups of membrane phospholipids have also recently been reported. Weber *et al.* observed tyrosine-choline cation-π interactions between Equinatoxin II and dodecylphosphocholine (DPC) and *N*-acetyl sphingomyelin micelles.[9] They used molecular dynamics (MD) simulations and the molecular mechanics Generalized Amber force field (GAFF).[10,11] We had earlier reported cation-π interactions between phosphatidylcholine (PC) head groups of dimyristoylphosphatidylcholine lipids (DMPC) and tyrosine amino acids of a bacterial phospholipase; *Bacillus thuringiensis* phosphatidylinositol-specific phospholipase C (*Bt*PI-PLC).[12] Cation-π adducts were also observed between tyrosine phenols and the DMPC choline groups in MD simulations with the additive CHARMM force field (CHARMM-ff).[13] Interestingly the occupancies of these interactions during the MD trajectory correlated qualitatively well with the effect the mutation of each of the tyrosines had on the experimentally measured affinity of the protein for DMPC vesicles. Furthermore the X-ray structure of a related bacterial PI-PLC resolved in the presence of choline or 1,2-dibutyryl-*sn*-glycero-3-phosphocholine (diC_4PC) confirmed the presence of cation-π interactions between the ligands and several tyrosines.[14]

Even though our earlier work indicates that the CHARMM-ff reproduces the tyrosine-choline (Tyr-Cho) interactions qualitatively well, the lack of explicit polarization or charge transfer effects generally raises the question of whether the structure and energetics of these interactions are quantitatively well modeled. Several studies have indeed shown that additive MM force fields capture the structures of cation-π adducts reasonably well however they are not adequate to accurately model the energetics of cation-π interactions.[15-17] Caldwell and Kollman showed that non-additive effects are important for accurate energetics of cation-π interactions involving benzene and proposed the use of a three-body term.[15]

Minoux and Chipot used quantum mechanics (QM) calculations on model systems to investigate the association of phenylalanine, tyrosine, and tryptophan with arginine and lysine. They found that induction contributes significantly and proposed a short-range 4-12 potential term as a cost effective solution to model the induction phenomena in cation-π interactions.[16] Felder *et al.* compared QM calculations with classical molecular mechanics calculations using the benzene-tetramethylammonium (TMA) complex and concluded that any existing force field could reproduce cation-π interactions reasonably with suitable modification of partial charges from quantum mechanical (QM) calculations.[17] The developments of polarizable force fields, such as AMOEBA[18] and the Drude polarizable force field (known as Drude Polarizable),[19,20] have obviously also brought improvements relevant to a more accurate description of cation-π interactions.[5]

Finding the most appropriate method to improve the modeling of any type of interaction by a MM force field requires an understanding of the nature of that interaction. Unfortunately none of the studies mentioned above has considered Tyr-Cho interactions and few quantum chemistry studies have focused on tetramethylammonium mediated cation-π interactions with phenol rings.[21] On the other hand, the nature of cation-π interactions mediated by benzene and cations have been widely investigated. Using self-consistent field calculations (SCF) Dougherty and co-workers showed that the electrostatic potential could be used as a qualitative tool to explain cation-π interaction between small cations (i.e. Na^+) and aromatic compounds when the cation is just above the aromatic ring.[22,23] This electrostatic potential model may work when the cation is bound to the aromatic ring mostly/solely via electrostatics. However, this model in principle works neither for polarization nor for dispersion effects. A series of studies by others demonstrated the role of polarization effect in cation-π interactions.[15,24-26] Soteras *et al.* showed the importance of polarization in cation-π interactions between alkali and alkaline earth metal cations and benzene.[25] Marshall *et al.* demonstrated that the off-axis contributions can be attractive, which is relevant for cases where the cation lies in the plane of the aromatic ring.[26] The authors studied benzene-cation complexes where the considered cations were Na^+, Li^+, K^+, and NH_4^+. Rapp *et al.* showed the effect of methylation of ammonium ions on interaction energies and geometries of methylated ammonium-benzene complexes where methylation decreases the strength of the cation-π interactions.[27] These works demonstrated that the nature of the cation-π interaction is not limited to electrostatics contributions and that studies should not be limited to the approach of the cations from above/below the aromatic ring. Moreover most of these studies do not consider solvation effects, which may be important for solution-phase cation-π interactions with relevance to the cellular environment.

We here report the study of a model system consisting of phenol and tetramethylammonium (TMA). We built the potential energy surface (PES) as a function of the distance between the two groups and of the approach angles. Different wave functions and density-functional based methods with various basis sets were benchmarked against large basis set CCSD(T) results. To evaluate the energetic contributions to the minima of the PES, we decomposed the energy using Symmetry Adapted Perturbation Theory (SAPT).[28] We also investigated the effect of solvation using the COSMO[29] model. We next compared the gas phase QM PES with the PES generated using both the CHARMM36 and Drude polarizable force fields. Finally, we propose a modified set of parameters for the CHARMM36 additive force field and show that its use in MD simulations of *Bt*PI-PLC bound to a DMPC bilayer improves the agreement between occupancies of cation-π interactions along the MD trajectory and experimental affinity data.

COMPUTATIONAL METHODS

1. Quantum mechanical calculations

1.1 Geometry optimization of the monomers

The monomers of phenol and TMA are optimized at the BLYP-D3 level with the cc-pVTZ basis set.[30] D3 represents the dispersion correction proposed by Grimme *et al.*[31] Structures were optimized until all gradients were smaller than 0.0003 au. The calculations were performed using NWCHEM (v. 6.3).[32]

1.2 Potential energy scans

The optimized monomers of phenol and TMA are used to build the phenol-TMA complex as shown in Figure 1. We build the PES as a function of R, θ and φ. We use the same set of reaction coordinates to obtain the PES at different levels of theory that will be compared. The X-axis is defined by the center of the phenol ring and the carbon atom carrying the OH group. **R** is the distance from the center of the phenol ring to the nitrogen atom of TMA, θ is the angle between the normal to the ring (or the Y-axis) and the distance vector **R.** φ is the angle between the X-axis and the projection of **R** in the XZ plane. The geometries of the complexes are not optimized as we perform rigid PES scanning. Complexes are built in such a way that three of the carbon atoms of TMA face the phenol for any given approach angle (tridentate configuration). Felder *et al.* showed that the tridentate configuration is more stable than the mono-dentate or bidentate configurations in the benzene-TMA complex.[17] Moreover the tridentate configuration is the most relevant for protein-phospholipid interactions, as the fourth choline carbon would be connected to the phosphate group.

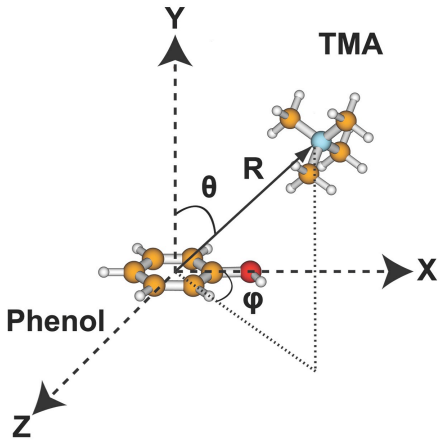

Figure 1. Phenol and tetramethylammonium (TMA) model system. The figure is generated using MOLDEN.[33]

1.3 Interaction energies

We performed single point energy calculations of the complex and the optimized monomers at different levels of theory and with various basis sets. Interaction energies are calculated as follows:

$$E_{\text{int}} = E_{AB} - (E_A + E_B) \quad (1)$$

where, AB: phenol-TMA complex, A: phenol and B: TMA.

The core orbitals C[1s], N[1s], O[1s] are kept frozen in the MP2 and CCSD(T) calculations. Basis set superposition errors (BSSE) for different levels of theory are calculated with the Counterpoise Correction approach.[34] All the interaction energies are corrected for BSSE.

As carrying out CCSD(T) calculations with large basis sets such as cc-pVQZ or cc-pV5Z is computationally very expensive even for a small system, we estimated the large basis set CCSD(T) (for cc-pVQZ or cc-pV5Z basis sets) energies from CCSD(T)/cc-pVTZ and large basis set MP2 calculations.[35] We denote this approach as cCCSD(T) in this manuscript. The procedure is as follows:

$$E_{cCCSD(T)/cc-pVQZ} \approx E_{CCSD(T)/cc-pVQZ}$$

$$\approx E_{MP2/cc-pVQZ} + (E_{CCSD(T)/cc-pVTZ} - E_{MP2/cc-pVTZ}) \quad (2)$$

The calculations were performed with the NWCHEM[32] (v6.3) program.

1.4 Interaction energy using SAPT and energy decomposition

We used wave function based Symmetry Adapted Perturbation Theory (SAPT) to evaluate interaction energies and to calculate the magnitude of the different contributions to the energies. All the SAPT calculations are performed using the PSI4 package (v 4.0b5).[36] Two variants of SAPT are used: SAPT0/aug-cc-pVDZ* and SAPT2+/aug-cc-pVDZ. The basis sets used for the SAPT0 calculations are truncated aug-cc-pVDZ basis sets and denoted as aug-cc-pVDZ* and the core orbitals were kept frozen. This choice of using different levels of SAPT methods also allows us to evaluate the reliability of SAPT variants for our system. The first one is known to give qualitative interaction energies at a relatively low computational cost[37] while the second one gives more quantitative interaction energies and is considered the silver standard for SAPT calculations.[37] We did not use the gold standard SAPT2+(3)δMP2/aug-cc-pVTZ, as we cannot assign the δMP2 correction to any physically meaningful energy components. For further details on the SAPT methods and the implementation in the PSI4 package, the reader is referred to excellent reviews elsewhere.[28,38]

1.5 Quantum solvation effect

We used the COSMO[29] solvation model to evaluate the effect of solvation on the PES. These calculations were performed using the BLYP functional[39,40] with a cc-pVTZ basis set using a dielectric constant of 78.4. The solvent interaction energy was calculated as follows:

$$E_{\text{int}}^{solv} = E_{\text{int}}^{SAPT\,2+} + \Delta G_{\text{int}}^{solv} \quad (3)$$

where

$$\Delta G_{\text{int}}^{solv} = \Delta G_{AB}^{solv} - (\Delta G_{A}^{solv} + \Delta G_{B}^{solv}) \quad (4)$$

AB, A and B represent the complex, phenol and TMA, respectively. Both the electrostatic and nonpolar components of the solvation free energy were considered. All COSMO solvation calculations were performed with the NWCHEM[32] (v 6.3) program.

2. Molecular mechanics calculations of the PES

Using the force fields we calculated interaction energies of the phenol-TMA complex in the same geometries as those used for the QM single point calculations. The parameters for phenol and TMA were taken from the CHARMM general force field (CGenFF) force field.[41] The MM interaction energies were calculated with NAMD[42] (v2.10) using no cut-off (mimicked by using a large cutoff value of 999 Å) for additive force fields. We performed the exact same calculations using the Drude polarizable force field.[19,20] We used the CHARMM[43] (v38b2) program for MM PES calculations using Drude polarizable force field. Calculations also used an infinite cutoff and at each step of the PES, the atomic coordinates were restrained with harmonic positional restraints (force constant: 100000 kcal/mol/Å^2) with the Drude particle positions optimized using the Steepest Descent minimizer to a gradient of 0.0001 kcal/mol/Å. This was performed on the dimer from which the energies of the fully optimized monomers were calculated as in equation 1 to give the interaction energy.

3. MD simulations of protein-membrane system

Bacillus thuringiensis PI-PLC (*Bt*PI-PLC) is a bacterial phospholipase. Using MD simulations with the additive CHARMM force field we have earlier shown that *Bt*PI-PLC anchored on a pure DMPC bilayer interacts with the phospholipids via cation-π interactions.[12] We here used a conformation extracted after 220ns of one of our earlier 500ns-long trajectories to launch one 100-ns long simulation with CHARMM-ff-mod and one with CHARMM-ff. All simulation parameters and analyses protocols are as described in Grauffel *et al.*[12] Briefly, using NAMD[42] (v2.10) the protein-bilayer system was simulated in the NPT ensemble using a 2 fs time step. The temperature of the system was set to 310 K and the temperature was controlled with Langevin dynamics using temperature-damping coefficient equal to 1.0. Pressure of the system was controlled using the Langevin piston method[44] setting the pressure to 1 atm, with an oscillation period of 200 fs, and a damping time scale of 50 fs. All bonds between hydrogen atoms and heavy atoms were constrained using the SHAKE algorithm.[45] The nonbonded interaction cutoff was set to 12 Å. We used switching functions for both the electrostatics and Lennard-Jones potentials with a switching distance set to 11 Å. The long-range electrostatics interactions beyond the cutoff were evaluated using Particle Mesh Ewald method.[46] We used the r-RESPA[47] multiple time step algorithm; short-range non-bonded forces were evaluated every 2 fs and long-range forces were evaluated every 4 fs.

For the RMSD calculations, the reference structure was the energy-minimized *Bt*PI-PLC structure in the presence of the bilayer. Cation-π interactions were defined between tyrosines and choline group of DMPC lipids if the two following criteria were met: (1) the nitrogen atom of the choline group was within 7 Å of all of the aromatic ring carbon atoms, and (2) the difference between these distances was within 1.5 Å.[16,48] The occupancies of these interactions were calculated as the ratio of the number of trajectory frames with the interactions present to the total number of frames.

RESULTS AND DISCUSSIONS

1. Benchmarking QM levels of theory

We first compare different QM levels of theory for TMA approaching perpendicularly to the aromatic plane, i.e. with approach angles (θ, φ)=(0°, 0°). Selected results are plotted in Figure 2 (see also Figures S1 to S3 for additional results). We start by comparing MP2 methods with various basis sets and find that at least a QZ basis set is necessary to have energy convergence to the basis limit (Cf. Figure S1). The interaction energies obtained by MP2/cc-pVQZ or MP2/cc-pV5Z levels nicely overlap (Cf. Figure2). Next, to evaluate the deviation between interaction energies calculated with density-functional based methods and those calculated with wave function based methods we performed the same calculations with the BLYP and B3LYP density functionals with dispersion correction. We then compared the DFT interaction energies to the CCSD(T) and MP2 results; there are significant differences near the energy minimum when using the cc-pVTZ basis set (Cf. Figure S2). Most notably, the CCSD(T) energies are lower (in absolute value) than the DFT and MP2 energies. When using a cc-pVQZ basis set, the MP2 interaction energies overlap with both BLYP-D3 and B3LYP-D3 interaction energies (Cf. Figure S3). However, they are still overestimated by ~1-1.5 kcal mol^{-1} compared to the CCSD(T) energies. The results of these comparisons using cc-pVTZ and cc-pVQZ basis sets reflect that interaction energies obtained using BLYP and B3LYP functionals are comparable, and that MP2 and DFT-based methods lead to a qualitative picture rather than a quantitative one. We also evaluated the performance of wave function-based SAPT variants (Cf. Figure 2) and find that it performs well for these approach angles, being closer to the CCSD(T) PES than to PES calculated with the MP2/cc-pVQZ or MP2/cc-pV5Z.

To summarize, for the perpendicular approach (θ=0°, φ=0°), the interaction energies obtained with the different methods can be sorted into three categories depending on how well they reproduce the minimum interaction energy obtained with large basis set CCSD(T); (i) MP2/cc-pVQZ, MP2/cc-pV5Z, BLYP-D3/cc-pVTZ, and BLYP-D3/cc-pVQZ overestimate the interaction energy, (ii) CCSD(T)/cc-pVTZ and SAPT0/aug-cc-pVDZ* underestimate it, (iii) SAPT2+/aug-cc-pVDZ nicely reproduces it. The interaction energy at the minima obtained by CCSD(T)/cc-pV5Z level (extrapolated) is -9.39 kcal mol^{-1} and SAPT2+/aug-cc-pVDZ level is -9.23 kcal mol^{-1}. Calculations using SCF methods (HF) largely underestimate the interaction energy (> 6 kcal mol^{-1}, data not shown). Due to the lack of electron correlation and hence dispersion, HF calculations are not reliable for this system. We would instead recommend MP2 or dispersion corrected DFT in cases where performing large basis set CCSD(T) calculations is impossible. One would thus obtain a reasonable qualitative overview of the PES.

We further compared different levels of theory for other approach angles, namely (θ,φ)=(45°,0°) and (90°,0°). For that purpose we calculated SAPT2+/aug-cc-pVDZ interaction energies and used those as reference values. In both cases, BLYP-D3 leads to an overestimation of the interaction energy (Cf. Figure S4 and Figure S5) independently from the number of functions in the basis set (cc-pVTZ, cc-pVQZ). Both MP2/cc-pVTZ and SAPT0/aug-cc-pVDZ* underestimate the interaction energies. Unlike when TMA approaches the phenol ring perpendicularly, i.e. (θ,φ)=(0°,0°), the MP2/cc-pVQZ interaction energies are very close to the SAPT2+/aug-cc-pVDZ values when the approach is either diagonal or parallel to the ring, i.e (θ,φ)=(45°,0°) and (90°,0°) respectively. This indicates that the triple excitation contribution is not significant for the off-axis approach.

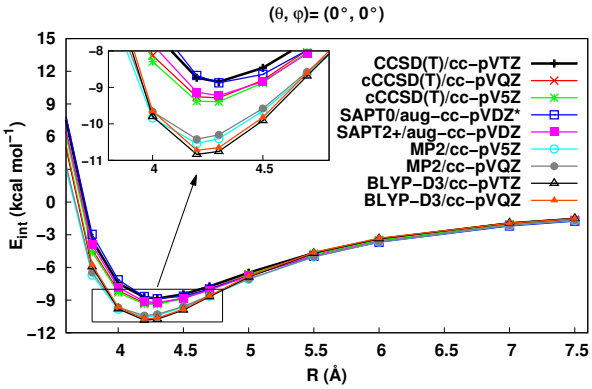

Figure 2. Interaction energies obtained using wave function based SAPT methods are compared to different levels of theory, both DFT and wave function based methods for phenol-TMA. SAPT2+/aug-cc-pVDZ nicely reproduces the large basis set CCSD(T) interaction energies.

2. SAPT2+/aug-cc-pVDZ PES and energy decomposition

Based on the benchmark above we chose to generate the PES using SAPT2+/aug-cc-pVDZ as reference and MP2/cc-pVQZ for all combinations of θ and φ angles listed in Table 1. The reason for using MP2 in addition to SAPT is two-fold. First of all, MP2 is widely used for the treatment of electron correlation and our benchmark results indicate that the MP2 interaction energies are reasonable also for the off-axis approach angles. Secondly, CHARMM force-field parameters are developed mostly using MP2 methods as reference for the calibration of bonded potentials parameters and, in selected cases, for the nonbonded terms.[19,41,49]

In what follows we focus on the SAPT2+ results while the MP2 results are presented and discussed in section 4. The analysis of the potential energy curves calculated with SAPT2+/aug-cc-pVDZ for the nine different pairs of (θ, φ) angles is summarized in Table 1. When the TMA approaches the phenol ring perpendicularly, (θ, φ)= (0°,0°), the contribution from dispersion is higher than the one from induction (Cf. Figure 3) and almost equal to the electrostatic contribution at the minima (Cf. Figure 3 and Table 1). When φ=90° the interaction energy at the minimum is influenced by the repulsion between the hydrogen atoms of TMA and the hydrogen atom of the hydroxyl group in phenol. Consequently, at equal θ, the minima at φ=90° are higher in energy than for other φ angles (Cf. Figure S6 (B) and Figure S7 (B)). For the in-plane approach directions (θ= 90°) the electrostatic contribution is favorable only when the hydroxyl oxygen can interact with the TMA, i.e. when φ=0° (Cf. Figure S7). For energy decompositions of other approach angles,

Table 1. SAPT2+/aug-cc-pVDZ interaction energies: minima location (R_{min}) and energy decomposition.

(θ, φ)[a]	R_{min}[b] (Å)	E_{int} (kcal mol^{-1})					Contribution to bonding energy[g] (%)		
		SAPT2+	ELEC[c]	EXCNG[d]	INDUC[e]	DISP[f]	ELEC	INDUC	DISP
0°,0°	4.3	-9.23	-6.54	7.58	-4.16	-6.10	38.93	24.78	36.29
45°,0°	5.3	-5.86	-3.96	6.20	-3.52	-4.58	32.82	29.15	38.02
45°,90°	5.2	-3.26	-0.74	4.15	-3.07	-3.60	9.95	41.45	48.60
45°,180°	5.0	-5.38	-3.17	5.83	-3.57	-4.46	28.32	31.88	39.80
45°,270°	5.2	-5.72	-3.15	4.01	-3.05	-3.54	32.33	31.32	36.35
90°,0°	6.7	-3.24	-0.60	2.72	-2.72	-2.64	10.00	45.66	44.34
90°,90°	6.0	0.06	3.10	1.42	-2.27	-2.18	N/A	50.99	49.01
90°,180°	5.8	-1.97	0.66	3.37	-2.93	-3.06	N/A	48.91	51.09
90°,270°	5.8	-3.01	-0.02	2.64	-2.74	-2.88	0.43	48.61	50.96

[a] Approach angles; [b] TMA-phenol distance at the interaction energy minimum; [c] electrostatics; [d] exchange; [e] induction; [f] dispersion; [g] bonding energy is defined as the sum of the favorable contributions to the binding energy

readers are referred to the supporting information (Cf. Figure S6 and Figure S7). Interestingly, dispersion plays a key role in any given approach angle that we considered as it always contributes more than 35% to the bonding energy. For the perpendicular approach of TMA with respect to the phenol ring (0°, 0°), dispersion and electrostatics are of comparable magnitude and larger than induction. For a diagonal approach (θ= 45°), dispersion becomes larger than both electrostatics and induction while for the in-plane approaches (θ=90°), electrostatics is mostly unfavorable while the favorable induction and dispersion terms are comparable. These energy decompositions show that dispersion plays a key role for the cation-π interaction between phenol and TMA. This is unlike what has been shown for other cations by Soteras *et al.*[25] and Marshall *et al.*[26] Marshall *et al.* further showed that the in-plane approach of Na^+ is electrostatically unfavorable but induction enables the cation to bind to benzene.[26] Readers are recommended to a review article by C. David Sherrill on energy components in π-interactions, particularly on polarization in cation-π interactions.[50] Cation-π interactions between benzene and TMA should also reflect a significant contribution from dispersion in principle. Indeed, the role of dispersion in the benzene-TMA[21,51] and phenol-TMA[21] complexes has been evaluated by calculating the energy difference between SCF and MP2 energy values but only for the perpendicular approach. Our energy decompositions of various approach angles for the benzene-TMA system confirm the significance of dispersion contributions (Cf. Section 6). However, we are not aware of previous reports of systematic energy decompositions results for the phenol-TMA complex and its PES. The systematic decomposition we report here can readily be used to improve and validate MM force field parameters. In terms of practical applications, this result is relevant for solution-phase supramolecular design that can take advantage of the contribution from dispersion implying a lesser susceptibility of this complex to solvent screening.

3. Solvent effect

To obtain a qualitative picture of the effect of solvation on phenol-TMA interactions, we used the COSMO solvation model. We performed single point energy calculations on the gas phase minima resulting from the calculations described in the previous section. Interaction energies in gas phase and in solution are listed in Table 2. Although the minima obtained from the in-plane approach directions (θ=90°) become unfavorable under the influence of a solvent, the minima along the perpendicular (θ=0°) and off-axis (θ=45°) directions remain favorable. The perpendicular approach yields the most favorable interaction energy, which is -3.33 kcal mol^{-1}. For the off-axis approaches (θ=45°), the most stabilizing interaction energy is -1.34 kcal mol^{-1} (Cf. Table 2).

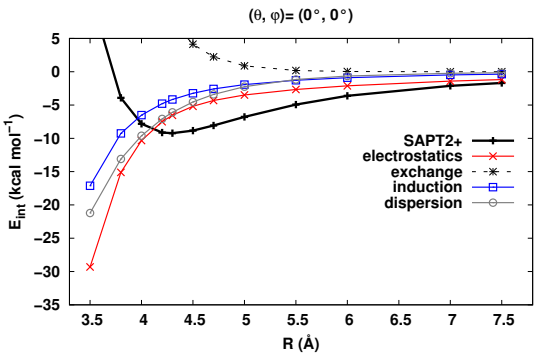

Figure 3. Energy decomposition using SAPT (SAPT2+/aug-cc-pVDZ) for phenol-TMA when (θ, φ)= (0°, 0°).

While PC lipids contain methylated ammonium groups others lipids such as phosphatidylethanolamine (PE) or phosphatidylserine (PS) contain ammonium groups. Further, amino acids other than tyrosine contain aromatic groups. In this respect it is interesting to compare phenol-TMA to phenol-$(NH_4)^+$ interactions and also to benzene-$(NH_4)^+$ interactions as it informs on the similarities/differences between tyrosine-PC interactions and tyrosine-PE or phenylalanine-PC interactions. Both phenol-$(NH_4)^+$ and benzene-$(NH_4)^+$ systems have been the subject of theoretical studies. Using CCSD(T) calculations Marshall *et al.* calculated interaction energies of -0.4 kcal mol^{-1} for benzene and ammonium in water,[26] and -16.4 kcal mol^{-1} in the gas phase. This is a slightly less favorable interaction energy than the -19 kcal mol^{-1} calculated by Rapp *et al.* using DFT (M06-2X/6-31++G**)[27] or the

-17.58 kcal mol^{-1} reported by Orabi *et al.*[52] using MP2(FC)/6-311++G(d,p). Interestingly, Rapp *et al.* showed that methylation decreases the interaction energy significantly with a value of -8.8 kcal mol^{-1} for the benzene-TMA complex. We also calculated the interaction energy for the benzene-TMA complex when TMA approaches perpendicularly to the aromatic ring of benzene using different levels of theory: -9.00 kcal mol^{-1} with SAPT2+/aug-cc-pVDZ, -10.13 kcal mol^{-1} with MP2/cc-pVQZ, and -10.18 with DFT BLYP-D3/cc-pVTZ at the energy minimum (Cf. Table S2, S3 and Figure S9). This is roughly the same magnitude as the one we obtained for the phenol-TMA interaction energies (-9.39 kcal mol^{-1} with CCSD(T)/cc-pV5Z and -10.65 kcal mol^{-1} with DFT BLYP-D3/cc-pVQZ level, Cf Figure 2), indicating that the presence of the hydroxyl group on the aromatic ring has less effect on the interaction than the presence of methyl groups on the nitrogen atom of the cation. While Marshall *et al.* calculated a dramatic effect (from -16.4 to -0.4 kcal mol^{-1}) of solvation on benzene-ammonium interactions, our results show that the effect is significantly smaller on phenol-TMA (from -9.23 to -3.33 kcal mol^{-1}) with interaction energies in solution being about eight times more favorable than for the benzene-ammonium complex. However, it was not clear if Marshall *et al.* included the nonpolar part of the solvation contribution for the benzene-ammonium complex.[26] We estimate from our calculations the nonpolar contributions to the benzene-ammonium interaction to be around -1 kcal mol^{-1}. Adding this to the value reported by Marshall *et al.*, we estimate the total interaction energy for the benzene-ammonium complex in water to be around -1.4 kcal mol^{-1}, which would still be significantly less than the -3.33 kcal mol^{-1} we obtain for phenol-TMA. We thus expect that cation-π interactions between aromatic amino acids and PC lipids would be stronger than with PE lipids in regions where the dielectric constant is high. Cheng *et al.* reported consistent results from binding experiments of protein to small unilamellar vesicles (SUV).[14] The authors showed that the binding to PG/PC SUVs is stronger than binding to PG/PE SUVs for an engineered protein where tyrosines were introduced to create choline binding sites.

Table 2. Effect of solvation on interaction energies of phenol-TMA gas phase minima (kcal mol^{-1}).

Approach angles (θ,φ)	R (Å)	Interaction energy (E_{int})	
		Gas phase[a]	Solvent model[b]
0°,0°	4.3	-9.23	-3.33
45°,0°	5.3	-5.86	-1.34
45°,90°	5.2	-3.26	-0.92
45°,180°	5.0	-5.38	-1.30
45°,270°	5.2	-5.72	-1.04
90°,0°	6.7	-3.24	0.01
90°,90°	6.0	0.06	0.36
90°,180°	5.8	-1.97	0.41
90°,270°	5.8	-3.01	0.24

[a]calculated at SAPT2+/aug-cc-pVDZ level; [b]calculated at BLYP/cc-pVTZ level using COSMO solvation model.

It is more difficult to compare tyrosine-PC interactions to phenylanine-PC interactions given the limited amount of data available but one could hypothesize from the interaction energies of phenol-TMA and benzene-TMA in the gas phase that the two complexes would have relatively comparable stability in water.

Given the importance of interactions between amino acids and membrane phospholipids it is relevant to consider the free energies of transfer of the phenylalanine and tyrosine side chains from water to the phospholipid bilayer. The transfer of a phenylalanine side chain to the center of a dioleoyl phosphatidylcholine (DOPC) bilayer has been calculated to be favorable (-3.1 kcal mol^{-1}) while that of a Tyr side chain is unfavorable (1.6 kcal mol^{-1}).[53,54] The free energies of transfer to the DOPC bilayer interface are favorable for both Phe and Tyr (-3.6 and -3.3 kcal mol^{-1}, respectively). Phenylalanine will have a greater tendency to insert towards the lipid tails than tyrosine. We thus believe that in the case of peripherally binding proteins or peptides, the probability of achieving cation-π interactions with PC lipids is greater for tyrosine than for phenylalanine.

4. Molecular mechanics PES: additive CHARMM36 vs Drude polarizable force fields

We calculated the gas phase TMA-phenol PES with both the additive CHARMM force field (CHARMM-ff) and the Drude polarizable force field. We report the identified minima and the interaction energies in Table 3 and compare them with the SAPT2+ results. The PES are compared in Figures 4 to 6.

Table 3. Location of energy minima, R_{min}(Å) and interaction energies, E_{int} (kcal mol^{-1}): results from SAPT2+/aug-cc-pVDZ, the CHARMM force field and the Drude polarizable force field.

Approach angles (θ, φ)	SAPT2+/aug-cc-pVDZ		Additive CHARMM36		Drude polarizable	
	R_{min}	E_{int}	R_{min}	E_{int}	R_{min}	E_{int}
0°,0°	4.3	-9.23	4.2	-6.97	4.2	-8.91
45°,0°	5.3	-5.86	5.5	-4.18	5.0	-5.15
45°,90°	5.2	-3.26	5.2	-0.14	5.0	-2.70
45°,180°	5.0	-5.38	5.0	-2.24	4.8	-6.58
45°,270°	5.2	-5.72	5.0	-4.59	4.9	-5.95
90°,0°	6.7	-3.24	6.7	-1.83	6.2	-3.01
90°,90°	6.0	0.06	N/A	N/A	5.5	0.34
90°,180°	5.8	-1.97	6.0	0.48	5.3	-3.73
90°,270°	5.8	-3.01	5.8	-2.51	5.5	-3.60

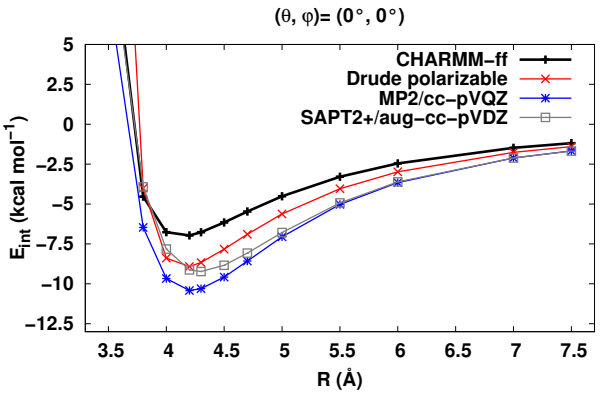

Figure 4. Comparison of gas phase QM PES and MM force field PES for TMA approaching perpendicularly to the phenol ring (θ, φ)=(0°, 0°).

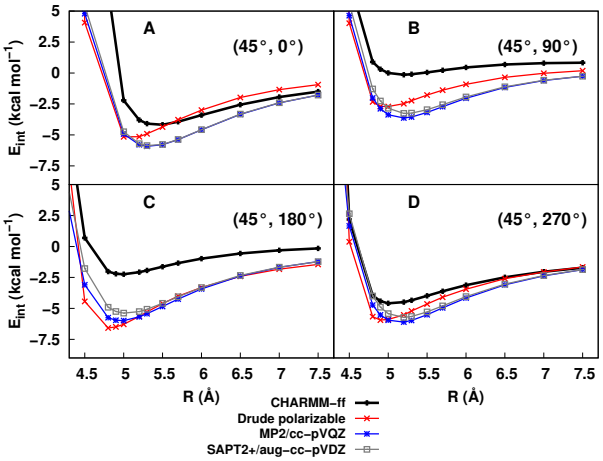

Figure 5. Comparison of gas phase QM PES and MM force field PES for TMA approaching diagonally (θ=45°, φ=0°, 90°, 180° or 270°).

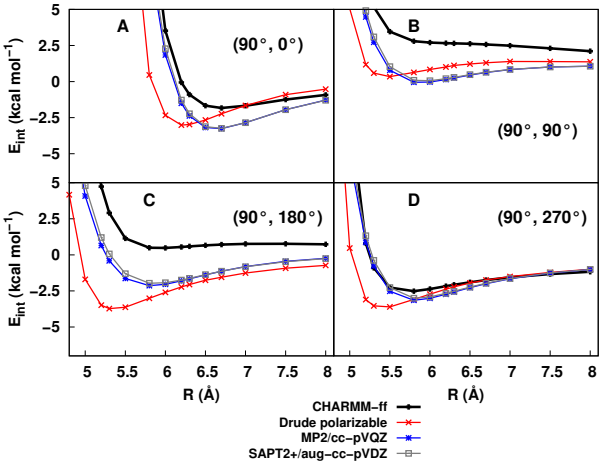

Figure 6. Comparison of gas phase QM PES and MM force field PES for TMA approaching in the plane of the aromatic ring (θ=90°, φ=0°, 90°, 180° or 270°).

The location of the minima calculated using the additive CHARMM force field is rather close to the location of the QM minima except for the approach angles (θ,φ)=(90°,90°). The CHARMM interaction energies are underestimated except for the approach angle (θ,φ)=(90°,270°). The use of the Drude polarizable force field significantly improves the interaction energies compared to the non-polarizable CHARMM force field even though they are slightly underestimated for angles φ=0°, 90° and overestimated for angles φ=180°. Yet it is worth noting that the Drude interaction energy at (θ, φ)=(0°, 0°) is closer to the CCSDT/cc-pV5Z value (-9.39 kcal mol^{-1}) than to the MP2/cc-pVQZ value (-10.42 kcal mol^{-1}). As discussed above, the latter has a tendency to overestimate the interaction energy. Overall the Drude force field tends to shift the minimum location towards the phenol (i.e. shorter distance between phenol and cation). While the phenol-TMA interaction is characterized by a rather large dispersion contribution, the improved agreement by the polarizable force field indicates the advantages of the explicit treatment of polarization for modeling cation-π interactions. This is consistent with the favorable contribution from induction observed in the SAPT decomposition analysis (Figure 3).

5. Improving the force field description of phenol-TMA cation-π interactions

With the nature of the phenol-TMA interaction in mind, we attempted to improve the force field by modifying the van der Waals terms by using pair-specific Lennard Jones (LJ) parameters.[55] In the CHARMM force-field nomenclature, these will be NBFIX terms, an approach that overcomes limitations in the use of the Lorentz-Berthelot combining rules. A major benefit of employing this approach is that all other interactions are unperturbed. We modified the pair-specific parameters of the LJ potential between the carbon atoms of the phenol ring and the carbon/nitrogen atoms of TMA. We modified the epsilon value while keeping the location of the minimum for these pairs unaltered. With such an approach, the location of the minimum (R_{min}) of the phenol-TMA complex is expected to remain close to the value obtained with CHARMM-ff. Our target was to reduce the energy difference (ca. -2.26 kcal mol^{-1}) between the target QM data and CHARMM-ff with the LJ interaction of 30 pairs of atoms. This provided us with an educated guess of the epsilon values, which we subsequently adjusted to best fit the reference PES. The incorporation of these additional interaction energies led to the reproduction of target QM data. The resulting force field is coined "CHARMM-ff-mod" in the remainder of the text. The NBFIX values used in CHARMM-ff-mod are listed in Table 4. The shapes of the resulting LJ potentials are compared to those without the correction i.e. CHARMM-ff in Figure S8.

Table 4. Pair-specific Lennard-Jones parameters (NBFIX terms) used in the modified CHARMM additive force field (CHARMM-ff-mod) compared to the CHARMM-ff. Atom types are presented inside the bracket.

NBFIX(cross-terms)	Epsilon (kcal mol^{-1})		Unaltered R(Å)
	CHARMM-ff	CHARMM-ff-mod	
C_{phenol}[a] – C_{TMA}[b]	-0.0734	-0.2081	4.2074

C_{phenol} – N_{TMA}[c]	-0.1183	-0.2400	3.8424

[a]C_{phenol} (CG2R61) [b]C_{TMA} (CG334) [c]N_{TMA} (NG3P0): corresponding atom types in CHARMM General force field

The reconstructed PESs are shown on Figures 7 to 9, where we also plot the PES obtained with the unmodified additive CHARMM-ff and with SAPT2+/aug-cc-pVDZ.

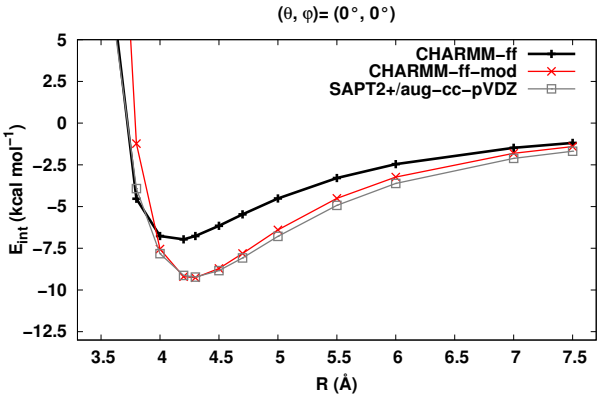

Figure 7. Effect of the modified LJ epsilon parameters on TMA-phenol molecular mechanics PES at (θ,φ)=(0°, 0°). Comparison between CHARMM-ff-mod (red line), CHARMM-ff (black line) and SAPT2+ (grey line).

With the pair-specific LJ terms in CHARMM-ff-mod, the reference interaction energy plots along several directions such as (θ,φ)=(0°,0°), (45°,0°), (45°,270°) are nicely reproduced (Cf. Figure 7 to 9). In particular, the difference between the QM and the MM energy minima at (θ,φ)=(0°,0°) is reduced from -2.26 with CHARMM-ff to 0.03 kcal mol^{-1} with CHARMM-ff-mod. For (θ,φ)=(90°,90°) while the CHARMM-ff fails to capture the minimum (Table 3, Figure 9B), CHARMM-ff-mod does capture a minimum at the same distance as the QM reference with R_{min}=5.8 Å (Table 5). The largest difference between QM and CHARMM-ff is observed for (θ,φ)=(45°, 180°) with -3.14 kcal mol^{-1} and is reduced to -1.51 kcal mol^{-1} with CHARMM-ff-mod. For the approach angles (θ,φ)=(90°,0°), (45°,180°) or (90°,180°) the interaction energies are still slightly underestimated with CHARMM-ff-mod while for (90°,270°) the interaction energies are slightly overestimated (Cf. Figure 9, A and D). For other approach angles, the PESs using the improved parameters show less deviation from QM reference than CHARMM-ff. Most importantly, the locations of the energy minima are comparable to the QM reference unlike what we observed with the Drude polarizable force field (Cf. Table 5). For the approach angles considered in our investigation, the mean absolute percentage error (MAPE) calculated between MM and QM interaction energies is around 50%, for CHARMM-ff while it is around 20% for Drude polarizable-ff and CHARMM-ff-mod (Cf. Table S1). However, the Drude polarizable-ff overestimates the equilibrium geometry by more than 5%. The CHARMM-ff-mod performs excellently with 0.5% MAPE in reproducing the equilibrium geometries. Average error for interaction energies are 2.0, -0.2, and 0.6 kcal mol^{-1} for CHARMM-ff, Drude polarizable-ff, and CHARMM-ff-mod, respectively. On the other hand, the average error for equilibrium geometries is 0.0 Å for both CHARMM-ff and CHARMM-ff-mod, whereas it is -0.3 Å for Drude polarizable-ff (Cf. Table S1).

Previous efforts to improve force field parameters for cation-π interactions were always limited to reproducing only the perpendicular approach of the cation towards aromatic rings.[15,16,52,56] In the present study we show that all approach angles need to be considered. This leads to overall improvement in the reproduction of the QM data along different approach directions, though the quality of the agreement does depend on the different directions (Cf. Table 3).

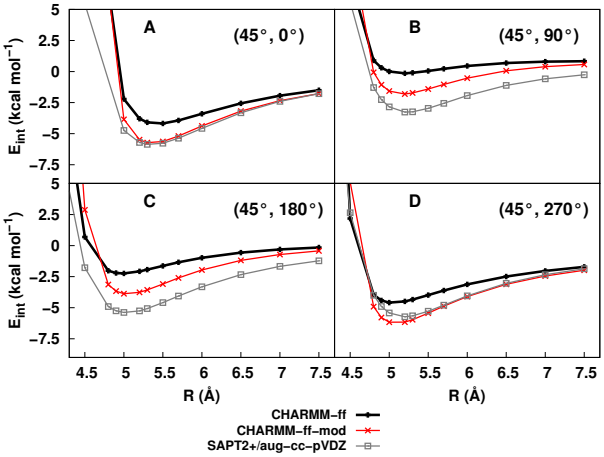

Figure 8. Effect of the modified LJ epsilon parameters on the TMA-phenol molecular mechanics PES for TMA approaching diagonally (θ=45°, φ=0°, 90°, 180° or 270°). Cf. legend of Figure 7.

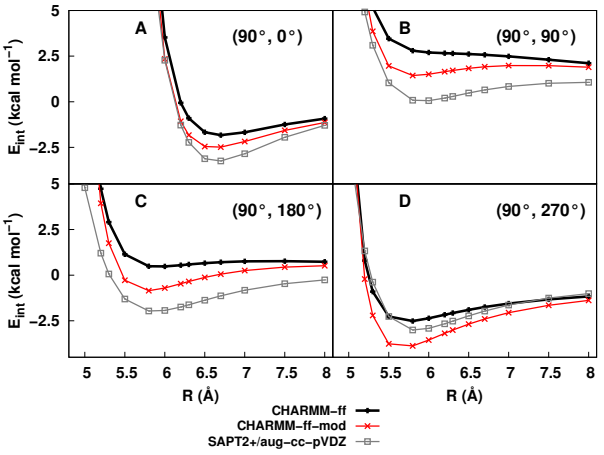

Figure 9. Effect of the modified LJ epsilon parameters on the TMA-phenol molecular mechanics PES TMA approaching in the plane of the aromatic ring (θ=90°, φ=0°, 90°, 180° or 270°). Cf. legend of Figure 7.

Table 5. Location and interaction energy of the energy minima obtained by the improved parameter set for CHARMM additive force field (CHARMM-ff-mod).

Approach angle	CHARMM-ff-mod	
	R_{min} (Å)	E_{int} (kcal mol^{-1})
0°,0°	4.3	-9.26
45°,0°	5.3	-5.72
45°,90°	5.2	-1.81

45°,180°	5.0	-3.87
45°,270°	5.0	-6.17
90°,0°	6.7	-2.49
90°,90°	5.8	1.43
90°,180°	5.8	-0.85
90°,270°	5.8	-3.88

6. Transferability of the proposed modified parameters for benzene-TMA interactions

The aromatic rings of tyrosine and phenylalanine are described using the same atom types in the CHARMM force field. To test the transferability of the modified parameter set (CHARMM-ff-mod) to benzene-TMA interactions; we compute the QM and MM PES for benzene-TMA. The computational procedures are the same as described for phenol-TMA interactions. Due to the symmetry of the benzene molecule, we considered only three pairs of approach angles (θ, φ)= [(0°, 0°), (45°, 0°), (90°, 0°)]. As observed for phenol-TMA, the MP2/cc-pVQZ and BLYP-D3/cc-pVTZ levels of theory overestimate the interaction energy for benzene-TMA interactions when the approach angles are (θ, φ)= (0°, 0°) (Cf. Figure S9). Energy decomposition (Cf. Figure S10) reveals similar trends for benzene-TMA as we observed for phenol-TMA interactions; the interaction energy is dominated by dispersion contributions (Cf. Table S2). Note that (θ, φ)= (45°, 0°) for benzene-TMA is comparable to (θ, φ)= (45°, 180°) of phenol-TMA; and (θ, φ)= (90°, 0°) for benzene-TMA is comparable to (θ, φ)= (90°, 180°) of phenol-TMA.

The comparison of reference QM data (SAPT2+/aug-cc-pVDZ) with the additive CHARMM force field shows that the interaction energies are underestimated for all the considered approach angles for benzene-TMA interactions (Cf. Figure S11 and Table S3). The comparison of potential energy curves obtained using CHARMM-ff-mod to the target QM data reveals a better agreement (Cf. Figure S11, Table S3 and S4). Error analysis on the obtained minima for CHARMM-ff and CHARMM-ff-mod reveals that the equilibrium geometries are nicely reproduced by both versions with a RMSD of 0.1 Å (Table S4). In terms of energy, CHARMM-ff has a RMSD of 1.8 kcal mol^{-1}. On the other hand, CHARMM-ff-mod has a RMSD of 0.4 kcal mol^{-1}. The mean absolute percentage error (MAPE) in terms of interaction energy is 48.9% for CHARMM-ff and it is 7.5% for CHARMM-ff-mod. These analyses reflect the better agreement of CHARMM-ff-mod with the target QM data and the improvement from CHARMM-ff. The proposed modified LJ parameters for phenol-TMA are thus readily transferable to benzene-TMA interactions.

Table 6. Cation-π interactions mediated by the tyrosine residues of *Bt*PI-PLC with pure DMPC bilayer.

Residues	Cation-π Occupancies (%)	
	CHARMM-ff	CHARMM-ff-mod
Y86	43.9	21.6
Y88	97.2	98.3
Y200	83.0	81.9
Y204	33.2	66.5
Y246	94.3	87.3
Y247	1.9	16.6
Y251	43.2	88.7

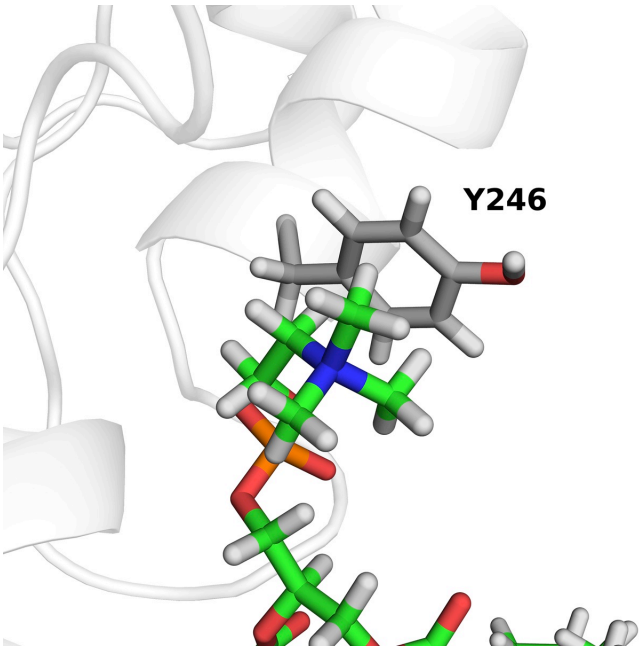

Figure 10. Cation-π interactions between Y246 of *Bt*PI-PLC. Y246 engages in long-lived cation-π interactions with a DMPC choline headgroups.

7. MD simulations of a bilayer-bound phospholipase

We compared the performance of CHARMM-ff and CHARMM-ff-mod in modeling interactions between a DMPC bilayer and the tyrosines of *Bt*PI-PLC. We performed a 100 nanosecond-long simulation of *Bt*PI-PLC on a DMPC bilayer with each parameter set. We do not observe significant differences in terms of protein structure stability or hydrophobic contacts and hydrogen bonds with bilayer lipids. The RMSDs of the protein backbone along the simulations are comparable with average values of 1.4±0.1 Å (CHARMM-ff) and 1.5±0.1 Å (CHARMM-ff-mod). The average numbers of hydrophobic contacts and hydrogen bonds mediated with the bilayer are, respectively, 47.9 and 13.0 when using CHARMM-ff, and 45.6 and 13.9 with CHARMM-ff-mod.

Analysis of cation-π interactions (Table 6 and Figure 10) shows that the tyrosine Y88, Y200, Y246 yield the highest occupancies along the trajectories with both CHARMM-ff and CHARMM-ff-mod. The occupancies of those cation-π interactions are well above 80% of the simulation time and comparable with both force fields. For Y204 and Y251 though we observe twice as high occupancies with CHARMM-ff-mod than with CHARMM-ff. On the other hand Y86 mediates less cation-π interactions with CHARMM-ff-mod than with the original FF. The occupancy of cation-π adducts

involving Y247, increases with CHARMM-ff-mod although it remains low and does not represent a stable cation-π interaction.

A

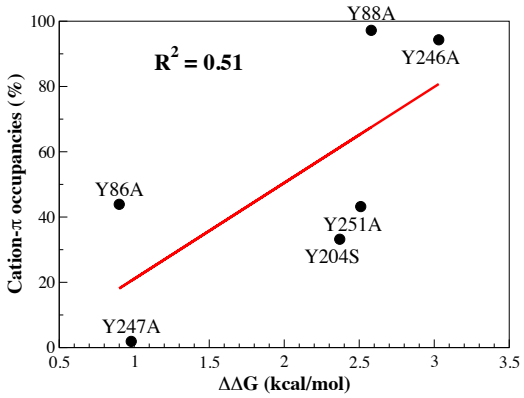

B

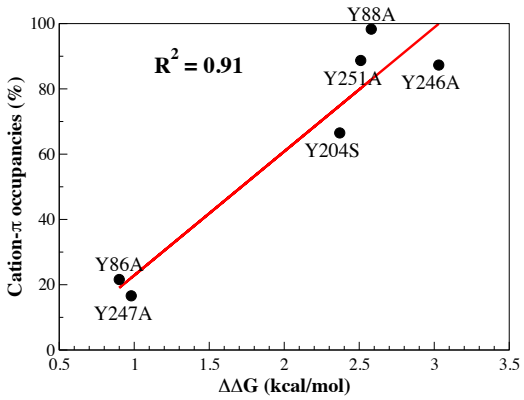

Figure 11. Comparison between occupancies of cation-π interactions observed during the MD simulations (100 ns) and evaluation of ΔΔG calculated from apparent K_d values measured by FCS for WT *Bt*PI-PLC and single tyrosine mutants. Both simulations and experiments are conducted with a DMPC bilayer. K_d and consequently ΔΔG values are taken from Grauffel *et al.*[12] The simulations are performed with (A) CHARMM-ff, and (B) CHARMM-ff-mod. R^2 values are calculated to assess the goodness of fit of the linear regressions.

We have earlier shown that the occupancies obtained from simulations with CHARMM-ff compared qualitatively well with experimentally determined ΔΔG values evaluated from the apparent K_d values of WT and Tyr to Ala mutations.[12] Experiments show that the affinity of tyrosine variants fall into two classes: (i) Y88, Y246, Y251 and Y204 whose mutation to alanine affected the K_d by 50-200 fold, corresponding to a ΔΔG of ca. 2.5 kcal mol^{-1} and (ii) Y86 and Y247A whose contribution to binding is estimated to be about 1 kcal mol^{-1} (See Grauffel *et al.*[12] for details). Figure 11 shows the cation-π occupancy vs ΔΔG plots for both force fields. With CHARMM-ff-mod we observe an excellent correlation between ΔΔG values and cation-π occupancies, which represents an improvement compared to CHARMM-ff notably with a better separation between the first and second class of tyrosines. This is demonstrated by R^2 = 0.91 with the CHARMM-ff-mod parameter set versus 0.51 with the original CHARMM-ff. These results show an improved ability of the new parameter set to model the relative strength of cation-π interactions between tyrosines and PC lipid bilayers.

CONCLUSION

In this work, we characterized the nature of the interaction between tyrosine and choline using the phenol-TMA complex as model system. Based on a benchmark of several QM levels of theory for that system we used SAPT2+/aug-cc-PVDZ to calculate a reference PES for phenol-TMA. We showed that the contribution from dispersion is of the same order of magnitude as that of electrostatics. Calculations using the COSMO solvation model show that the effect of solvent is smaller than what has been estimated for phenol-ammonium complexes. We further benchmarked the additive CHARMM36 and the Drude polarizable force fields against our QM reference PES and observed that CHARMM underestimates the interaction energies while the Drude polarizable force field performs significantly better in terms of interaction energies but slightly over- or underestimates the distances at the minimum energy. We showed that the use of pair-specific Lennard-Jones parameters in which the epsilon values between tyrosine ring carbons and choline carbon and nitrogen atoms are made more favorable yields better reproduction of those distance obtained with QM calculations. Importantly, this parameter set yields increased occupancy of Tyr-choline interactions in MD simulations of a bilayer-bound bacterial phospholipase, and yields improved agreement with affinity data on tyrosine mutants. The use of the NBFIX approach to implement the modification makes utilization of the new parameter set straightforward as NBFIX is also available in programs such as NAMD, GROMACS and OpenMM. The force field modification is thus easily available for MD simulations.

ASSOCIATED CONTENT

Supporting Information. Four Tables: error analysis for phenol-TMA (Table S1), energy decomposition for benzene-TMA (Table S2), comparison of QM PES (MP2/cc-pVQZ) and MM force field PES (CHARMM-ff, CHARMM-ff-mod) energy minima for benzene-TMA (Table S3), and error analysis for benzene-TMA (Table S4).
11 Figures: benchmark results for QM levels of theory for phenol-TMA (Figure S1-S5), energy decompositions of phenol-TMA for different approach angles (Figure S6 and S7), shape of LJ potentials (Figure S8), benchmark results of benzene-TMA for QM levels of theory (Figure S9), energy decompositions of benzene-TMA for different approach angles (Figure S10), comparison of gas phase QM PES and MM force field PES for benzene-TMA (Figure S11). This material is available free of charge via the Internet at http://pubs.acs.org.

AUTHOR INFORMATION

Corresponding Author

* NR: Universitetet i Bergen, Molekylaerbiologisk institutt, Pb. 7803 N-5020 Bergen, nathalie.reuter@uib.no.

Author Contributions

The manuscript was written through contributions of all authors. All authors have given approval to the final version of the manuscript.

Funding Sources

N.R. and H.M.K.: Norwegian Research Council (FRIMEDBIO #214167 and FRIMEDBIO #251247). ADM Jr.: National Institutes of Health (GM070855 and GM072558).

ACKNOWLEDGMENTS

NOTUR (Norwegian metacenter for computational science, project number #4700k) is thankfully acknowledged for provision of CPU time.

ABBREVIATIONS

PC, phosphatidylcholine; TMA, tetramethylammonium; PES, potential energy surface; QM, quantum mechanics; SAPT, symmetry adapted perturbation theory; MD, molecular dynamics.

REFERENCES

(1) Gallivan, J. P.; Dougherty, D. A. *Proc. Natl. Acad. Sci.* **1999**, *96*, 9459.

(2) Dougherty, D. A. *J. Nutr.* **2007**, *137*, 1504S.

(3) Dougherty, D. A. *Science* **1996**, *271*, 163.

(4) Ma, J. C.; Dougherty, D. A. *Chem. Rev.* **1997**, *97*, 1303.

(5) Zheng, X.; Wu, C.; Ponder, J. W.; Marshall, G. R. *J. Am. Chem. Soc.* **2012**, *134*, 15970.

(6) Kamps, J. J. A. G.; Huang, J.; Poater, J.; Xu, C.; Pieters, B. J. G. E.; Dong, A.; Min, J.; Sherman, W.; Beuming, T.; Matthias Bickelhaupt, F.; Li, H.; Mecinovic, J. *Nat. Commun.* **2015**, *6*.

(7) Sussman, J. L.; Harel, M.; Frolow, F.; Oefner, C.; Goldman, A.; Toker, L.; Silman, I. *Science* **1991**, *253*, 872.

(8) Xiu, X.; Puskar, N. L.; Shanata, J. A. P.; Lester, H. A.; Dougherty, D. A. *Nature* **2009**, *458*, 534.

(9) Weber, D. K.; Yao, S.; Rojko, N.; Anderluh, G.; Lybrand, T. P.; Downton, M. T.; Wagner, J.; Separovic, F. *Biophys. J.* **2015**, *108*, 1987.

(10) Abel, S.; Dupradeau, F.-Y.; Marchi, M. *J. Chem. Theory Comput.* **2012**, *8*, 4610.

(11) Wang, J.; Wolf, R. M.; Caldwell, J. W.; Kollman, P. A.; Case, D. A. *J. Comput. Chem.* **2004**, *25*, 1157.

(12) Grauffel, C.; Yang, B.; He, T.; Roberts, M. F.; Gershenson, A.; Reuter, N. *J. Am. Chem. Soc.* **2013**, *135*, 5740.

(13) MacKerell, A. D.; Bashford, D.; Bellott; Dunbrack, R. L.; Evanseck, J. D.; Field, M. J.; Fischer, S.; Gao, J.; Guo, H.; Ha, S.; Joseph-McCarthy, D.; Kuchnir, L.; Kuczera, K.; Lau, F. T. K.; Mattos, C.; Michnick, S.; Ngo, T.; Nguyen, D. T.; Prodhom, B.; Reiher, W. E.; Roux, B.; Schlenkrich, M.; Smith, J. C.; Stote, R.; Straub, J.; Watanabe, M.; Wiórkiewicz-Kuczera, J.; Yin, D.; Karplus, M. *J. Phys. Chem. B* **1998**, *102*, 3586.

(14) Cheng, J.; Goldstein, R.; Gershenson, A.; Stec, B.; Roberts, M. F. *J. Biol. Chem.* **2013**, *288*, 14863.

(15) Caldwell, J. W.; Kollman, P. A. *J. Am. Chem. Soc.* **1995**, *117*, 4177.

(16) Minoux, H.; Chipot, C. *J. Am. Chem. Soc.* **1999**, *121*, 10366.

(17) Felder, C.; Jiang, H.-L.; Zhu, W.-L.; Chen, K.-X.; Silman, I.; Botti, S. A.; Sussman, J. L. *J. Phys. Chem. A* **2001**, *105*, 1326.

(18) Ponder, J. W.; Wu, C.; Ren, P.; Pande, V. S.; Chodera, J. D.; Schnieders, M. J.; Haque, I.; Mobley, D. L.; Lambrecht, D. S.; DiStasio, R. A.; Head-Gordon, M.; Clark, G. N. I.; Johnson, M. E.; Head-Gordon, T. *J. Phys. Chem. B* **2010**, *114*, 2549.

(19) Vanommeslaeghe, K.; MacKerell, A. D. *Biochim. Biophys. Acta, Gen. Subj.* **2015**, *1850*, 861.

(20) Lopes, P. E. M.; Huang, J.; Shim, J.; Luo, Y.; Li, H.; Roux, B.; MacKerell, A. D. *J. Chem. Theory Comput.* **2013**, *9*, 5430.

(21) Pullman, A.; Berthier, G.; Savinelli, R. *J. Am. Chem. Soc.* **1998**, *120*, 8553.

(22) Mecozzi, S.; West, A. P.; Dougherty, D. A. *J. Am. Chem. Soc.* **1996**, *118*, 2307.

(23) Mecozzi, S.; West, A. P.; Dougherty, D. A. *Proc. Natl. Acad. Sci.* **1996**, *93*, 10566.

(24) Cubero, E.; Luque, F. J.; Orozco, M. *Proc. Natl. Acad. Sci.* **1998**, *95*, 5976.

(25) Soteras, I.; Orozco, M.; Luque, F. J. *Phys. Chem. Chem. Phys.* **2008**, *10*, 2616.

(26) Marshall, M. S.; Steele, R. P.; Thanthiriwatte, K. S.; Sherrill, C. D. *J. Phys. Chem. A* **2009**, *113*, 13628.

(27) Rapp, C.; Goldberger, E.; Tishbi, N.; Kirshenbaum, R. *Proteins: Struct., Funct., Bioinf.* **2014**, *82*, 1494.

(28) Jeziorski, B.; Moszynski, R.; Szalewicz, K. *Chem. Rev.* **1994**, *94*, 1887.

(29) Klamt, A.; Schüürmann, G. *J. Chem. Soc., Perkin Trans. 2* **1993**, 799.

(30) Dunning, T. H. *J. Chem. Phys.* **1989**, *90*, 1007.

(31) Grimme, S.; Antony, J.; Ehrlich, S.; Krieg, H. *J. Chem. Phys.* **2010**, *132*, 154104.

(32) Valiev, M.; Bylaska, E. J.; Govind, N.; Kowalski, K.; Straatsma, T. P.; Van Dam, H. J. J.; Wang, D.; Nieplocha, J.; Apra, E.; Windus, T. L.; de Jong, W. A. *Comput. Phys. Commun.* **2010**, *181*, 1477.

(33) Schaftenaar, G.; Noordik, J. H. *J. Comput.-Aided Mol. Des.* **2000**, *14*, 123.

(34) Boys, S. F.; Bernardi, F. *Mol. Phys.* **1970**, *19*, 553.

(35) Pitoňák, M.; Janowski, T.; Neogrády, P.; Pulay, P.; Hobza, P. *J. Chem. Theory Comput.* **2009**, *5*, 1761.

(36) Turney, J. M.; Simmonett, A. C.; Parrish, R. M.; Hohenstein, E. G.; Evangelista, F. A.; Fermann, J. T.; Mintz, B. J.; Burns, L. A.; Wilke, J. J.; Abrams, M. L.; Russ, N. J.; Leininger, M. L.; Janssen, C. L.; Seidl, E. T.; Allen, W. D.; Schaefer, H. F.; King, R. A.; Valeev, E. F.; Sherrill, C. D.; Crawford, T. D. *WIREs Comput Mol Sci* **2012**, *2*, 556.

(37) Parker, T. M.; Burns, L. A.; Parrish, R. M.; Ryno, A. G.; Sherrill, C. D. *J. Chem. Phys.* **2014**, *140*, 094106.

(38) Hohenstein, E. G.; Sherrill, C. D. *WIREs Comput Mol Sci* **2012**, *2*, 304.

(39) Becke, A. D. *Phys. Rev. A* **1988**, *38*, 3098.

(40) Lee, C.; Yang, W.; Parr, R. G. *Phys. Rev. B* **1988**, *37*, 785.

(41) Vanommeslaeghe, K.; Hatcher, E.; Acharya, C.; Kundu, S.; Zhong, S.; Shim, J.; Darian, E.; Guvench, O.; Lopes, P.; Vorobyov, I.; Mackerell, A. D. *J. Comput. Chem.* **2010**, *31*, 671.

(42) Phillips, J. C.; Braun, R.; Wang, W.; Gumbart, J.; Tajkhorshid, E.; Villa, E.; Chipot, C.; Skeel, R. D.; Kalé, L.; Schulten, K. *J. Comput. Chem.* **2005**, *26*, 1781.

(43) Brooks, B. R.; Brooks, C. L.; Mackerell, A. D.; Nilsson, L.; Petrella, R. J.; Roux, B.; Won, Y.; Archontis, G.; Bartels, C.; Boresch, S.; Caflisch, A.; Caves, L.; Cui, Q.; Dinner, A. R.; Feig, M.; Fischer, S.; Gao, J.; Hodoscek, M.; Im, W.; Kuczera, K.; Lazaridis, T.; Ma, J.; Ovchinnikov, V.; Paci, E.; Pastor, R. W.; Post, C. B.; Pu, J. Z.; Schaefer, M.; Tidor, B.; Venable, R. M.; Woodcock, H. L.; Wu, X.; Yang, W.; York, D. M.; Karplus, M. *J. Comput. Chem.* **2009**, *30*, 1545.

(44) Feller, S. E.; Zhang, Y.; Pastor, R. W.; Brooks, B. R. *J. Chem. Phys.* **1995**, *103*, 4613.

(45) Andersen, H. C. *J. Comput. Phys.* **1983**, *52*, 24.

(46) Essmann, U.; Perera, L.; Berkowitz, M. L.; Darden, T.; Lee, H.; Pedersen, L. G. *J. Chem. Phys.* **1995**, *103*, 8577.

(47) Izaguirre, J. s. A.; Reich, S.; Skeel, R. D. *J. Chem. Phys.* **1999**, *110*, 9853.

(48) Petersen, F. N. R.; Jensen, M. Ø.; Nielsen, C. H. *Biophys. J.* **2005**, *89*, 3985.

(49) Mackerell, A. D. *J. Comput. Chem.* **2004**, *25*, 1584.

(50) Sherrill, C. D. *Acc. Chem. Res.* **2013**, *46*, 1020.

(51) Kim, K. S.; Lee, J. Y.; Lee, S. J.; Ha, T.-K.; Kim, D. H. *J. Am. Chem. Soc.* **1994**, *116*, 7399.

(52) Orabi, E. A.; Lamoureux, G. *J. Chem. Theory Comput.* **2012**, *8*, 182.

(53) MacCallum, J. L.; Bennett, W. F. D.; Tieleman, D. P. *J. Gen. Physiol.* **2007**, *129*, 371.
(54) MacCallum, J. L.; Bennett, W. F. D.; Tieleman, D. P. *Biophys. J.* **2008**, *94*, 3393.
(55) Baker, C. M.; Lopes, P. E. M.; Zhu, X.; Roux, B.; MacKerell, A. D. *J. Chem. Theory Comput.* **2010**, *6*, 1181.
(56) Ansorg, K.; Tafipolsky, M.; Engels, B. *J. Phys. Chem. B* **2013**, *117*, 10093.

For Table of Contents Only

Improving the force field description of tyrosine-choline cation-π interactions: QM investigation of phenol-N(Me)$_4^+$ interactions

Hanif M. Khan, Cédric Grauffel, Ria Broer, Alexander D. MacKerell Jr., Remco W. A. Havenith, and Nathalie Reuter